Zus, F., Deng, Z., Wickert, J. (2017): The impact of higher-order ionospheric effects on estimated tropospheric parameters in Precise Point Positioning. - *Radio Science*, *52*, 8, pp. 963—971.

DOI: http://doi.org/10.1002/2017RS006254

AGU PUBLICATIONS

Radio Science

RESEARCH ARTICLE
10.1002/2017RS006254

**Key Points:**
- Simulations reveal that higher-order ionospheric effects have a significant impact on the estimated tropospheric parameters in PPP
- Ionospheric corrections must be consistently applied in PPP and the orbit and clock generation

**Correspondence to:**
F. Zus,
zusflo@gfz-potsdam.de

**Citation:**
Zus, F., Z. Deng, and J. Wickert (2017), The impact of higher-order ionospheric effects on estimated tropospheric parameters in Precise Point Positioning, *Radio Sci.*, *52*, 963–971, doi:10.1002/2017RS006254.

Received 20 JAN 2017
Accepted 26 JUL 2017
Accepted article online 29 JUL 2017
Published online 15 AUG 2017



# The impact of higher-order ionospheric effects on estimated tropospheric parameters in Precise Point Positioning

**F. Zus[1], Z. Deng[1], and J. Wickert[1]**

[1]German Research Centre for Geosciences, Potsdam, Germany

**Abstract** The impact of higher-order ionospheric effects on the estimated station coordinates and clocks in Global Navigation Satellite System (GNSS) Precise Point Positioning (PPP) is well documented in literature. Simulation studies reveal that higher-order ionospheric effects have a significant impact on the estimated tropospheric parameters as well. In particular, the tropospheric north-gradient component is most affected for low-latitude and midlatitude stations around noon. In a practical example we select a few hundred stations randomly distributed over the globe, in March 2012 (medium solar activity), and apply/do not apply ionospheric corrections in PPP. We compare the two sets of tropospheric parameters (ionospheric corrections applied/not applied) and find an overall good agreement with the prediction from the simulation study. The comparison of the tropospheric parameters with the tropospheric parameters derived from the ERA-Interim global atmospheric reanalysis shows that ionospheric corrections must be consistently applied in PPP and the orbit and clock generation. The inconsistent application results in an artificial station displacement which is accompanied by an artificial "tilting" of the troposphere. This finding is relevant in particular for those who consider advanced GNSS tropospheric products for meteorological studies.

## 1. Introduction

When the Global Navigation Satellite System signals traverse the Earth's atmosphere they are affected by the ionosphere and neutral atmosphere [*Hartmann and Leitinger*, 1984]. The first-order ionospheric effect, which is the main contributor (99.9%) to the signal phase advance (group delay), is removed by forming the linear combination of dual-frequency observables. The remaining higher-order ionospheric effects are caused by higher-order terms in the refractive index for the phase (group) of the signal and raypath bending [*Hoque and Jakowski*, 2008]. Typically, the higher-order ionospheric effects are modeled using idealized electron density fields. *Kashcheyev et al*. [2012] used a realistic electron density field to highlight that for a ground-based station the higher-order ionospheric effects show both a strong elevation and a strong azimuth angle dependency.

The impact of the higher-order ionospheric effects on the estimated geodetic parameters of ground-based stations was subject to numerous studies. *Kedar et al*. [2003] found that the application of higher-order ionospheric corrections leads to a southwards shift of stations. However, since satellite parameters were held fixed, their analysis forced the higher-order ionospheric corrections to be absorbed solely by the station parameters. Later *Fritsche et al*. [2005], who estimated both station and satellite parameters, showed that the majority of the higher-order ionospheric correction is absorbed by the satellite parameters. A recent study by *Garcia-Fernandez et al*. [2013] utilizes Precise Point Positioning (PPP) [*Zumberge et al*., 1997]. They show that ionospheric corrections must be consistently applied in PPP and the orbit and clock product generation. The inconsistent application results in an artificial station displacement. In all studies little attention has been paid to the impact of higher-order ionospheric effects on the estimated tropospheric parameters. This is probably due to the fact that tropospheric parameters (the tropospheric zenith delays and gradient components) are considered nuisance parameters in geodesy. However, tropospheric parameters are considered a data source for meteorological studies [*Bevis et al*., 1992, *Bar-Sever et al*., 1998, *Douša et al*. [2016]].

The purpose of the present work is to reveal how higher-order ionospheric effects leak into estimated tropospheric parameters in PPP. We introduce the basic observable, the modeling of higher-order ionospheric effects, and perform an idealized simulation. The following practical example shows under which circumstances and to what extent the quality of tropospheric parameters is affected. We use Numerical Weather Model (NWM) derived tropospheric parameters for that purpose.

The structure of this paper is as follows. In section 2 we introduce the observation equation. In section 3 we describe the higher-order ionospheric effects. In section 4 we show how the higher-order ionospheric effects leak into estimated tropospheric parameters. The conclusion is given in section 5.

## 2. Observation Equation

The observation equation for some satellite station link is written as

$$\phi_i = \rho + T - I_i + c{\cdot}t + m_i{\cdot}\lambda_i \tag{1}$$

where the left-hand side includes the measured accumulated phase between the satellite and the station $\phi i$ and the right-hand side includes the geometric distance $\rho$, the tropospheric delay $T$, the ionospheric delay $Ii$, the station clock error $t$, and the integer number $mi$ of wavelengths $\lambda i$. The subscript $i$ denotes the carrier frequency and $c$ denotes the vacuum speed of light. Multipath effects and measurement noise are ignored. The observation equation above is valid for phase measurements. A similar observation equation can be obtained for code measurements.

We note that the observation equation can be written as

$$\phi_i = O_i + c{\cdot}t + m_i{\cdot}\lambda_i \tag{2}$$

where $Oi$ denotes the optical path length

$$O_i = \rho + T - I_i \tag{3}$$

## 3. Higher-Order Ionospheric Effects

The refractive index experienced by the phase of the radio signal is approximated by

$$n_i = 1 + 10^{-6}N - \frac{40.3}{f_i^2}N_e - \frac{1.1284{\cdot}10^{12}}{f_i^3}B{\cdot}\cos(\theta){\cdot}N_e \tag{4}$$

where $N$ denotes the refractivity of the neutral atmosphere, $fi$ denotes the carrier frequency, $\theta$ is the angle between the Earth's magnetic field vector $\boldsymbol{B}$ and the wave normal vector, and $Ne$ denotes the electron density [*Moore and Morton*, 2011]. For the considered carrier frequencies, the wave normal vector can be approximated by the ray-tangent vector ("quasi-isotropic" approximation). Then the optical path length reads as

$$O_i = \int\left(1 + 10^{-6}N - \frac{40.3}{f_i^2}N_e - \frac{1.1284{\cdot}10^{12}}{f_i^3}B{\cdot}\cos(\theta){\cdot}N_e\right)ds_i \tag{5}$$

where $dsi$ denotes the line element of the raypath. The tropospheric delay reads as

$$T = \int\left(1 + 10^{-6}N\right)ds{-}\rho \tag{6}$$

where $ds$ denotes the line element of the raypath in the absence of the ionosphere. Therefore, the ionospheric delay reads as

$$I_i = \int\left(1 + 10^{-6}N\right)\,ds - \int\left(1 + 10^{-6}N - \frac{40.3}{f_i^2}N_e - \frac{1.1284{\cdot}10^{12}}{f_i^3}B{\cdot}\cos(\theta){\cdot}N_e\right)ds_i \tag{7}$$

The raypaths follow from Fermat's principle.

In this study the raypaths and ray-integrals are computed utilizing the algorithm described by *Zus et al.* [2017]. The underlying electron density field is provided from a climatological model, the International Reference Ionosphere (IRI) [*Bilitza*, 2001]; Earth's magnetic field is provided from the 12th generation of International Geomagnetic Reference Field (IGRF) [*Matteo and Morton*, 2011]; and the refractivity field of the neutral atmosphere is provided from the ERA-Interim reanalysis [*Dee et al.*, 2011]. For a given station location and time we compute ionospheric delays (the elevation angles are 3°, 5°, 7°, 10°, 15°, 20°, 30°, 50°, 70°, and 90°, and the spacing in azimuth is 30°) and store them in a look-up table. The ionospheric delay for an arbitrary elevation and azimuth angle is obtained by interpolation. Tropospheric delays are computed as well, and the derived zenith delays, Mapping Function (MF) coefficients, and gradient components are stored in

a second look-up table [*Zus et al*., 2015a, 2015b]. Hence, for some elevation angle *e* and azimuth angle *a*, the tropospheric delay can be assembled according to

$$T(e,a) = m_h(e)\cdot Z_h + m_w(e)\cdot Z_w + m_g(e)[\cos(a)\cdot G_n + \sin(a)\cdot G_e] \tag{8}$$

where *Zh* denotes the zenith hydrostatic delay, *Zw* denotes the zenith wet delay, *mh* denotes the hydrostatic MF, *mw* denotes the wet MF, *mg* denotes the gradient MF [*Bar-Sever et al*., 1998], *Gn* denotes the north-gradient component, and *Ge* denotes the east-gradient component. The gradient components will be used at a later stage for comparison purposes.

The standard linear combination of dual-frequency observables

$$\phi = \frac{f_1^2}{f_1^2 - f_2^2}\phi_1 - \frac{f_2^2}{f_1^2 - f_2^2}\phi_2 = \rho + T - \delta I + c\cdot t + A \tag{9}$$

removes first-order ionospheric effects The ambiguity term *A* reads as

$$\mathrm{A} = \frac{f_1^2}{f_1^2 - f_2^2} m_1\cdot\lambda_1 - \frac{f_2^2}{f_1^2 - f_2^2} m_2\cdot\lambda_2 \tag{10}$$

The ionospheric residual $\delta I$ reads as

$$\delta I = \frac{f_1^2}{f_1^2 - f_2^2} I_1 - \frac{f_2^2}{f_1^2 - f_2^2} I_2 = \delta I_1 + \delta I_2 + \delta I_3 \tag{11}$$

where

$$\begin{aligned} \delta I_1 &= \frac{1.1284\cdot 10^{12}}{f_1^2 - f_2^2}\left(\frac{1}{f_1}\int B\cdot\cos(\theta)\, N_e\, ds_1 - \frac{1}{f_2}\int B\cdot\cos(\theta)\, N_e\, ds_2\right) \\ \delta I_2 &= \frac{40.3}{f_1^2 - f_2^2}\left(\int N_e\, ds_1 - \int N_e\, ds_2\right) \\ \delta I_3 &= \int\left(1 + 10^{-6}N\right)ds - \left(\frac{f_1^2}{f_1^2 - f_2^2}\int\left(1 + 10^{-6}N\right)ds_1 - \frac{f_2^2}{f_1^2 - f_2^2}\int\left(1 + 10^{-6}N\right)ds_2\right) \end{aligned} \tag{12}$$

The ionospheric residual $\delta I$ is not sensitive to the refractivity of the neutral atmosphere *N*. Specifically, if the troposphere is neglected $N = 0$ implies $ds = d\rho$; $ds1$ and $ds2$ are the line elements of the raypaths when the troposphere is neglected and the three terms agree with those provided by *Kashcheyev et al*. [2012]. In essence, the third term $\delta I3$ is caused by the raypath bending, the second term $\delta I2$ is due to the fact that the raypath bending is different for different carrier frequencies, and the first term $\delta I1$ is caused by the Earth's magnetic field. We do not study the three terms separately as this was already done in detail by *Kashcheyev et al*. [2012]. We examine the (total) ionospheric residual $\delta I$ which is obtained from the look-up table.

As an example we select a single station which is located in Potsdam (Germany) and show in Figure 1 the ionospheric residual as a function of time in 2012 (medium solar activity). For simplicity for each month values from only 1 day (the 15th day of the month) are shown. Each day consists of 12 epochs (2 h resolution) in UTC. Figure 1 (top)shows the ionospheric residual for the elevation angle 90°. Figure 1 (middle and bottom)shows the ionospheric residual for the elevation angle 7° and the azimuth angle 0° and 180°, respectively. By taking into account that the measurement noise is typically about 4 mm (the measurement noise is amplified by forming the standard linear combination) the ionospheric residuals are significant. This is not only true for low-elevation angles (Figure 1, middle and bottom) but also in the zenith direction (Figure 1, top). Clearly, the ionospheric residuals depend on the time of the day: high around noon and low around midnight. Therefore, we anticipate the largest impact of the ionospheric residual on the estimated tropospheric parameters around noon.

## 4. Results and Discussion

### 4.1. Simulation

We mimic PPP and show how the ionospheric residuals leaks into estimated station coordinates, clocks, and tropospheric parameters. To do so, we utilize the linearized observation equation

$$\delta I(e,a) = -u(e,a)\cdot\delta X + m_w(e)\cdot\delta Z_w + m_g(e)[\cos(a)\cdot\delta G_n + \sin(a)\cdot\delta G_e] + c\cdot\delta t \tag{13}$$

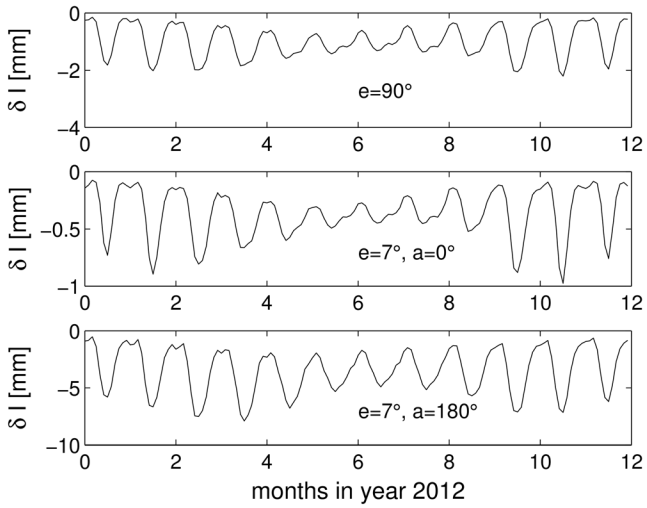


**Figure 1.** The ionospheric residual as a function of the time in the year 2012 for the station Potsdam (Germany). Each month consists of 1 day only (the 15th day of each month). Each day consists of 12 epochs (2 h resolution) in UTC. T(top) The ionospheric residual in the zenith direction. (middle and bottom) The ionospheric residual for the elevation angle 7° and the azimuth angle 0° (180°).

where $\boldsymbol{u}$ denotes the tangent-unit vector of the station-satellite link, $\delta\boldsymbol{X}$ denotes the coordinate residual, $\delta t$ denotes the clock residual, $\delta Gn$ denotes the north gradient residual, $\delta Ge$ denotes the east gradient residual, and $\delta Zw$ denotes the zenith delay residual. For simplicity the ambiguity term is ignored. For a single epoch we consider 144 station satellite links where azimuth angles are selected randomly and elevation angles are obtained through $e = 90–83\sqrt{r}$ where $r\in[0,1]$ is obtained from a random number generator. The set of station satellite links mimics a realistic observation geometry with a cutoff elevation angle of 7°. The respective ionospheric residuals $\delta I$ are obtained from the look-up tables. For each day we consider the four epochs 3, 9, 15, and 21 UTC. Then we combine the four sets of equations and obtain by a least squares fit the coordinate residuals on a daily basis and the clock and tropospheric parameter residuals epoch wise. The standard elevation angle-dependent weighting sin($e$) is applied in the least squares fit. In essence, the linearized observation equations are written as

$$\delta\mathbf{l} = \boldsymbol{J}\,\delta\mathbf{v} \tag{14}$$

where the vector $\delta\boldsymbol{l}$ includes the ionospheric residuals for the individual station satellite links, $\boldsymbol{J}$ denotes the Jacobian matrix, and the vector $\delta\boldsymbol{v}$ includes the coordinate residual (daily) and the clock and tropospheric parameter residuals (epoch wise). This equation is inverted to yield the vector $\delta\boldsymbol{v}$ given the vector $\delta\boldsymbol{l}$

$$\delta\mathbf{v} = \left(\boldsymbol{J}^T\,\boldsymbol{W}\,\boldsymbol{J}\right)^{-1}\boldsymbol{J}^T\,\boldsymbol{W}\;\;\delta\mathbf{l} \tag{15}$$

The weight matrix $\boldsymbol{W}$ reads as

$$W_{kl} = \sin(e_k)\;\sin(e_l)\delta_{kl} \tag{16}$$

where the subscript indices denote the individual station satellite links. We select a few hundred stations with good global coverage (the station locations are indicated in the figures below) and the month March in 2012. Finally, for each station and separately for each epoch we compute the monthly average and standard deviation of the residuals. We note that the monthly standard deviations are negligibly small compared to the monthly averages. This can be explained by the fact that the state of the ionosphere strongly depends on the year (solar activity), time of the day (day/night), and the season. The day-to-day variability is comparably weak.

In the positioning and timing domain the results agree qualitatively and quantitatively with results from previous studies [*Kedar et al*., 2003]. In essence, the ionospheric residual leads to a southward shift of the stations (not shown). As regard to the tropospheric parameter domain we do not analyze each epoch separately. We anticipate that the largest impact of the ionospheric residuals on the estimated tropospheric parameters is around noon and therefore focus on the single epoch 15 LT. Hence, for each station we select the epoch closest to 15 LT. The scatterplot in Figure 2 shows the station specific monthly average of the zenith delay residual at 15 LT. The zenith delay residuals are negligibly small close to the poles, tend to be negative elsewhere, and reach about −1.5 mm at low latitudes (around the geomagnetic equator). To put these numbers into perspective; the standard deviation between GPS and NWM zenith delays is typically about 10 mm at midlatitudes and 15 mm around the equator [*Li et al*., 2015]. The scatterplot in Figure 3 shows the station specific monthly average of the east-gradient residual at 15 LT. The east-gradient residuals, which depend on

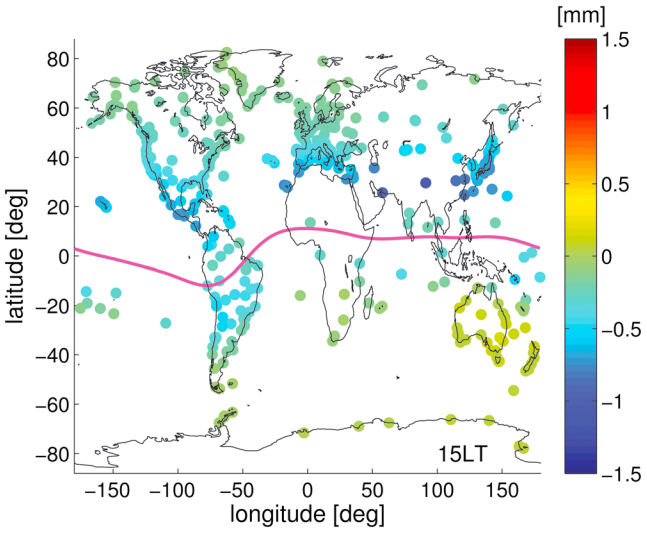


**Figure 2.** Scatterplot showing the station specific monthly average of the zenith delay residual at 15 LT (march 2012). The geomagnetic equator (line in magenta) is shown as well.

longitude rather than on latitude, reach ±0.05 mm. For comparison, the standard deviation between GPS and NWM east-gradient components is typically about 0.5 mm [*Douša et al.*, 2016]. Finally, the scatterplot in Figure 4 shows the station specific monthly average of the north-gradient residual at 15 LT. The north-gradient residuals show a latitude dependency. By taking into account that the standard deviation between GPS and NWM north-gradient components is typically about 0.5 mm [*Douša et al.*, 2016], the north gradient residuals of 0.2 mm are highly significant. In essence, the simulation study shows that in the tropospheric parameter domain it is in particular the north-gradient component that is affected. This is due to the strong correlation between the estimated station north coordinate and the north gradient component (see linearized observation equation above).

In practice (see next section) a simplified ionospheric residual is used. The ionospheric residual is based on the thin shell approximation for the ionosphere. This means that raypath bending is not taken into account and all electrons are assumed to be concentrated at a single thin shell at an altitude of 450 km. The simplified ionospheric residual $\delta I_s$ can be written as

$$\delta I_s(e,a) = -\frac{1.1284\cdot 10^{12}}{f_1 f_2 (f_1+f_2)} B(e,a)\cdot \cos(\theta(e,a))\cdot M(e)\cdot V(e,a) \tag{17}$$

where $V$ denotes the vertical total electron content (VTEC) and $M$ denotes the single-layer model MF [*Schaer*, 1999]. All quantities in the expression above are evaluated at the point where the straight line between the station and the satellite hits the altitude 450 km. The respective VTEC can be computed from the IRI. Since in the simulation (this section) the (rigorous) ionospheric residual $\delta I$ is used and in practice (see next section) the simplified ionospheric residual $\delta I_s$ is used, it is worthwhile to examine the difference of the coordinate, clock, and tropospheric parameter residual

$$\begin{aligned}\Delta\delta\mathbf{v} &= \delta\mathbf{v} - \delta\mathbf{v}_s \\ &= \left(\mathbf{J}^T\mathbf{W}\mathbf{J}\right)^{-1}\mathbf{J}^T\mathbf{W}\ \left(\delta\mathbf{l} - \delta\mathbf{l}_s\right)\end{aligned} \tag{18}$$

The scatterplot in Figure 5 shows the difference for the north gradient residual at 15 LT. The application of the ionospheric residual $\delta I$ instead of the simplified ionospheric residual $\delta I_s$ increases the north gradient residual to the north of the geomagnetic equator (up to +0.05 mm) and

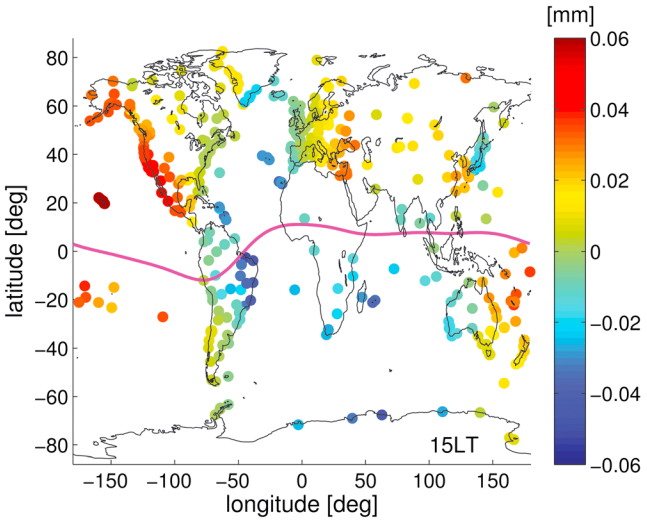


**Figure 3.** Scatterplot showing the station specific monthly average of the east gradient residual at 15 LT (march 2012). The geomagnetic equator (line in magenta) is shown as well.

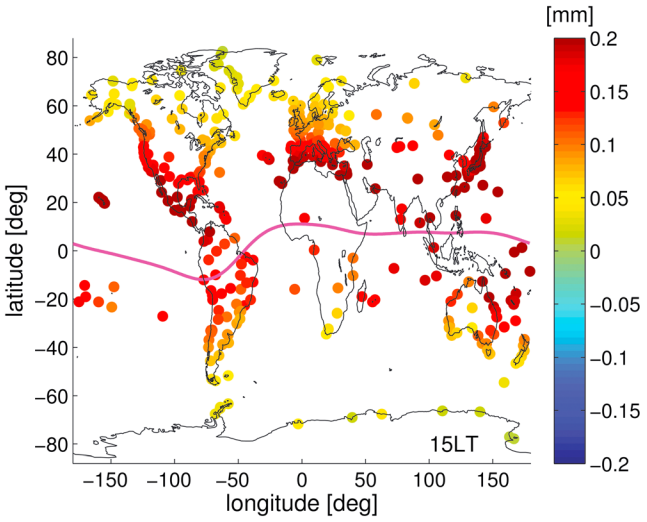


**Figure 4.** Scatterplot showing the station specific monthly average of the north gradient residual at 15 LT (march 2012). The geomagnetic equator (line in magenta) is shown as well.

decreases the north gradient residual to the south of the geomagnetic equator (up to −0.05 mm). This effect can be explained by the raypath bending. Let us consider a station located 20° to the north of the geomagnetic equator: signals arriving from the south of the station experience significant raypath bending (the signals traverse the equatorial anomaly), whereas signals arriving from the north of station experience little raypath bending (the signals traverse regions of low electron density). The correction of this asymmetric effect yields an increased north gradient component. Conversely, let us consider a station located 20° to the south of the geomagnetic equator: signals arriving from the north of the station will experience significant raypath bending (they traverse the equatorial anomaly) whereas signals arriving from the south of station will experience little raypath bending (the signals traverse regions of low electron density). The correction of this asymmetric effect yields a decreased north gradient component. However, this effect caused by the raypath bending is comparable small as it reaches only about 25% of the net effect shown in Figure 4. Therefore, for the purpose of this study, the application of the simplified ionospheric residual in practice (see next section) is deemed adequate.

### 4.2. Practice

We select the same stations and time period and apply/do not apply higher-order ionospheric corrections in PPP. The ionospheric residual is modeled as usual by the thin shell approximation for the ionosphere. Earth's magnetic field is provided from the IGRF, and the VTEC is provided from the Center for Orbit Determination in Europe Global Ionospheric Map. We generate our own orbits and clocks [*Deng et al.*, 2016]. We consider solely satellites from the Global Positioning System (GPS). In PPP the station coordinates are estimated on a daily basis, station clock errors are estimated epoch by epoch, zenith delays are estimated on a hourly basis, and gradients are estimated on a two-hourly basis. In the tropospheric delay model we use the hydrostatic and wet VMF1 [*Boehm et al.*, 2006] and the gradient MF as proposed by *Bar-Sever et al.* [1998]. The cutoff elevation angle is 7°, and the standard elevation angle-dependent weighting is applied. Then we calculate the difference between the tropospheric parameters (ionospheric corrections

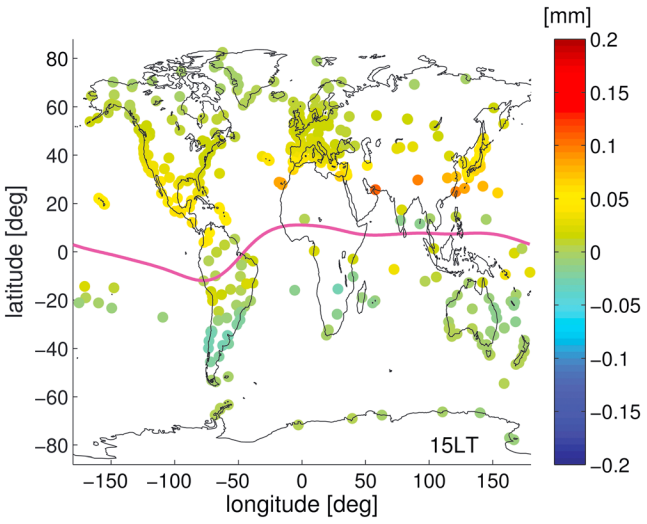


**Figure 5.** Scatterplot showing the difference of the station specific monthly average of the north gradient residual at 15 LT (march 2012) when different ionospheric residuals are applied. For details refer to the text. The geomagnetic equator (line in magenta) is shown as well.

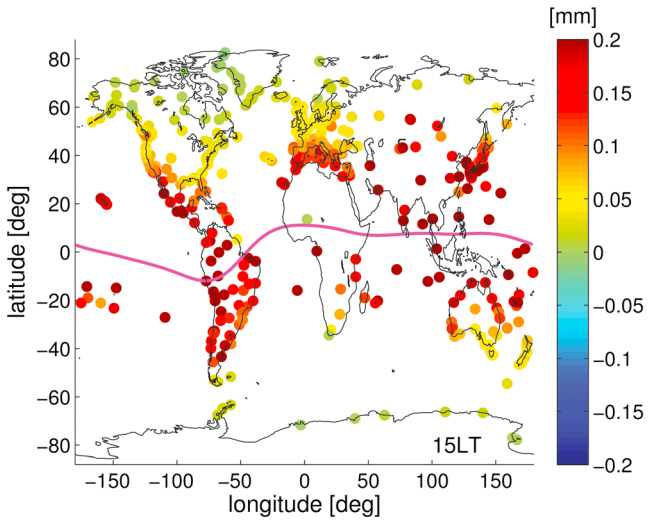


**Figure 6.** Higher-order ionospheric corrections are applied/not applied in PPP. Scatterplot showing the station specific monthly average of the north gradient residual at 15 LT (march 2012). The geomagnetic equator (line in magenta) is shown as well.

applied minus ionospheric corrections not applied), and for each station and separately for each epoch we calculate the monthly average and standard deviation of the residuals. Again, we find that the monthly standard deviations are negligibly small compared to the monthly averages.

The scatterplot in Figure 6 shows the station specific monthly average of the north gradient residual at 15 LT. Figure 6 can be compared to Figure 4, and an overall good agreement can be stated. In essence, the north gradient residuals show a latitude dependency and reach about 0.2 mm. The discrepancies between Figures 6 and 4 are due to the idealized assumptions in the simulation. We also note that the ionospheric residual that is used in the simulation is somewhat different from the ionospheric residual that is used in the experiment. For example, the raypath bending effects are taken into account in the simulation, whereas they are not taken into account in the experiment. As shown in Figure 5 the raypath bending effects can increase (decrease) the north gradient residuals to the north (south) of the geomagnetic equator by about 25%.

Finally, we compare the north gradient components with the north gradient components derived from the ERA-Interim reanalysis to assess whether ionospheric corrections should be applied in PPP. At this stage it is necessary to specify if ionospheric corrections are applied in the orbit and clock generation [*Garcia-Fernandez et al.*, 2013]. We consider the four possibilities; (1) ionospheric corrections are applied in the orbit and clock generation, and they are applied in PPP; (2) ionospheric corrections are applied in the orbit and clock generation, but they are not applied in PPP; (3) ionospheric corrections are not applied in the orbit and clock generation, and they are not applied in PPP; and (4) ionospheric corrections are not applied in the orbit and clock generation, but they are applied in PPP.

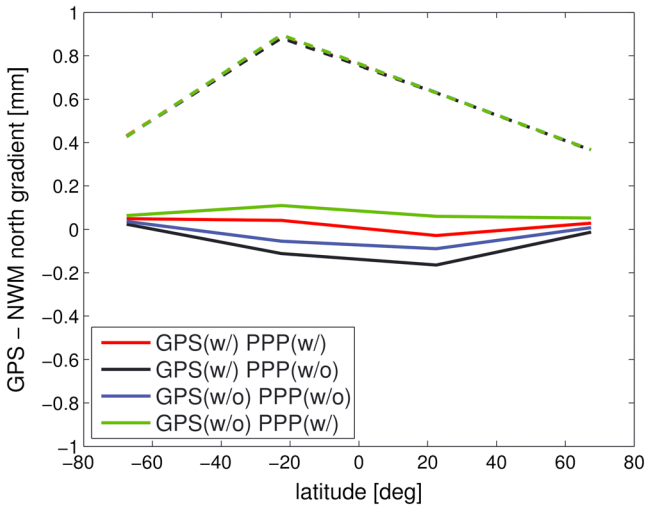


**Figure 7.** The mean and standard deviation between GPS and ERA-Interim north gradient components as a function of the latitude at 15 LT (March 2012). The solid (dashed) lines correspond to the mean (standard) deviation. The different colors correspond to the four possible combinations in the processing; with higher-order ionospheric corrections or without higher-order ionospheric corrections.

The mean and standard deviation between GPS and ERA-Interim north gradient components as a function of the latitude at 15 LT are shown in Figure 7. The different colors correspond to the four possibilities described above. The dashed (solid) line corresponds to the standard (mean) deviation. At first we note that the standard deviations for the four possibilities are nearly indistinguishable, whereas the mean

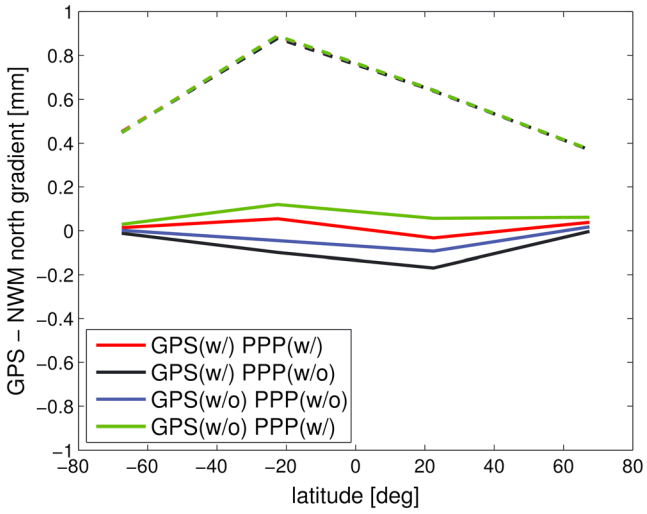


**Figure 8.** Same as in Figure 7 but ERA-Interim is replaced by GFS.

deviations for the four possibilities are different. The inconsistent application of ionospheric corrections leads to a positive (negative) mean deviation. The sign of the mean deviation depends on the implementation. In case the ionospheric corrections are consistently applied, the mean deviation is closer to zero. In case the ionospheric corrections are consistently not applied, the mean deviation is closer to zero as well. The NWM north gradient components cannot be regarded error free. In order to check to what extent the results are accidental in this respect we compare the north gradient components with the north gradient components derived from a different NWM, the Global Forecast System (GFS) operational analysis (www.ncep.noaa.gov). The mean and standard deviation between GPS and GFS north gradient components as a function of the latitude at 15 LT are shown in Figure 8. The standard deviations shown in Figure 8 are slightly larger than the standard deviations shown in Figure 7 which is probably due to the fact that an atmospheric reanalysis (ERA-Interim) is more accurate than an atmospheric operational analysis (GFS). More importantly, the mean deviations shown in Figure 8 closely match the mean deviations shown in Figure 7. Hence, both NWMs lead to the same conclusion, and this conclusion is in line with the results from *Garcia-Fernandez et al.* [2013]; ionospheric corrections must be consistently applied in PPP and the orbit and clock generation.

## 5. Conclusions

We performed a simulation study for 1 month in 2012 (medium solar activity) to reveal the potential impact of higher-order ionospheric effects on estimated tropospheric parameters in PPP around noon. The simulation study includes hundreds of stations with good global coverage. The impact is significant for all tropospheric parameters, zenith delays, and gradients, if we consider the typical formal error estimates in PPP. From the perspective of an independent data source, i.e., from a NWM, the impact is significant in particular for the north-gradient component. This is the case for almost all station locations except for those close to the poles. This result might be relevant for those who consider the gradients or derived products, i.e., the tropospheric delays assembled from zenith delays and gradients, for meteorological studies.

Therefore, in a practical example we select the same stations and time period and apply/do not apply ionospheric corrections in PPP. We generate our own orbits and clocks. We compare the two sets of tropospheric parameters (ionospheric corrections applied/not applied) and find an overall good agreement with the prediction from the simulation study. The comparison of the tropospheric parameters with the tropospheric parameters derived from NWMs suggests that ionospheric corrections should not be applied in PPP when they are not applied in the orbit and clock generation. This result is in line with the results from literature; ionospheric corrections must be consistently applied in PPP and the orbit and clock product generation. The inconsistent application results in an artificial station displacement and an artificial "tilting" of the troposphere.

The net effect of ionospheric corrections on estimated tropospheric parameters (differences when ionospheric corrections are applied in both, the orbit and clock generation and PPP, or neither) is small at least for the short time period studied here. It will be necessary to study a long time period (a number of solar cycles), and it will be worthwhile to consider a more sophisticated model for the ionospheric correction than the one that is used in our practical example, e.g., the one that is used in the simulation. This will be subject to a future study.

**Acknowledgments**
The IRI data are available at http://iri.gsfc.nasa.gov/. The IGRF data are available at http://www.ngdc.noaa.gov/IAGA/vmod/igrf.html. The ERA-interim data are available at the European Centre for Medium-Range Weather Forecast (http://www.ecmwf.int/en/research). The GFS data are provided by the National Centers for Environmental Prediction (www.ncep.noaa.gov). The look-up tables for the ionospheric delays and tropospheric delay parameters are available at ftp://ftp.gfz-potsdam.de/pub/home/kg/zusflo/ION/LUT/. The IGS products are available at https://igscb.jpl.nasa.gov/components/prods.html.

## References

Bar-Sever, Y. E., P. M. Kroger, and J. A. Borjesson (1998), Estimating horizontal gradients of tropospheric path delay with a single GPS receiver, *J. Geophys. Res.*, *103*(B3), 5019–5035, doi:10.1029/97JB03534.

Boehm, J., B. Werl, and H. Schuh (2006), Troposphere mapping functions for GPS and very long baseline interferometry from European Centre for Medium-Range Weather Forecasts operational analysis data, *J. Geophys. Res.*, *111*, B02406, doi:10.1029/2005JB003629.

Bevis, M., S. Businger, T. A. Herring, C. Rocken, R. A. Anthes, and R. H. Ware (1992), GPS meteorology: Remote sensing of atmospheric water vapor using the global positioning system, *J. Geophys. Res.*, *97*(D14), 15,787–15,801, doi:10.1029/92JD01517.

Bilitza, D. (2001), International Reference Ionosphere 2000, *Radio Sci.*, *36*(2), 261–275, doi:10.1029/2000RS002432.

Dee, D. P., et al. (2011), The ERA-Interim reanalysis: Configuration and performance of the data assimilation system, *Q. J. R. Meteorol. Soc.*, *137*, 553–597, doi:10.1002/qj.828.

Deng, Z., G. Gendt, and T. Schöne (2016), Status of the TIGA tide gauge data reprocessing at GFZ, in *IAG 150 Years: Proceedings of the IAG Scientific Assembly in Postdam, Germany, 2013*, *International Association of Geodesy Symposia*, vol. 143, edited by C. Rizos and P. Willis, pp. 33–40, Springer Int., Cham.

Douša, J., G. Dick, M. Kačmařík, R. Brožková, F. Zus, H. Brenot, A. Stoycheva, G. Möller, and J. Kaplon (2016), Benchmark campaign and case study episode in central Europe for development and assessment of advanced GNSS tropospheric models and products, *Atmos. Meas. Tech.*, *9*, 2989–3008, doi:10.5194/amt-9-2989-2016.

Fritsche, M., R. Dietrich, C. Knöfel, A. Rülke, S. Vey, M. Rothacher, and P. Steigenberger (2005), Impact of higher-order ionospheric terms on GPS estimates, *Geophys. Res. Lett.*, *32*, L23311, doi:10.1029/2005GL024342.

Garcia-Fernandez, M., S. D. Desai, M. D. Butala, and A. Komjathy (2013), Evaluation of different approaches to modeling the second-order ionospheric delay on GPS measurements, *J. Geophys. Res. Space Physics*, *118*, 7864–7873, doi:10.1002/2013JA019356.

Hartmann, G. K., and R. Leitinger (1984), Range errors due to ionospheric and tropospheric effects for signal frequencies above 100 MHz, *Bull. Geod.*, *58*, 109–136, doi:10.1007/BF02520897.

Hoque, M. M., and N. Jakowski (2008), Estimate of higher order ionospheric errors in GNSS positioning, *Radio Sci.*, *43*, RS5008, doi:10.1029/2007RS003817.

Kashcheyev, A., B. Nava, and S. M. Radicella (2012), Estimation of higher-order ionospheric errors in GNSS positioning using a realistic 3-D electron density model, *Radio Sci.*, *47*, RS4008, doi:10.1029/2011RS004976.

Kedar, S., G. A. Hajj, B. D. Wilson, and M. B. Heflin (2003), The effect of the second order GPS ionospheric correction on receiver positions, *Geophys. Res. Lett.*, *30*(16), 1829, doi:10.1029/2003GL017639.

Li, X., F. Zus, C. Lu, G. Dick, T. Ning, M. Ge, J. Wickert, and H. Schuh (2015), Retrieving of atmospheric parameters from multi-GNSS in real time: Validation with water vapor radiometer and numerical weather model, *J. Geophys. Res. Atmos.*, *120*, 7189–7204, doi:10.1002/2015JD023454.

Matteo, N. A., and Y. T. Morton (2011), Ionospheric geomagnetic field: Comparison of IGRF model prediction and satellite measurements 1991–2010, *Radio Sci.*, *46*, RS4003, doi:10.1029/2010RS004529.

Moore, R. C., and Y. T. Morton (2011), Magneto-ionic polarization and GPS signal propagation through the ionosphere, *Radio Sci.*, *46*, RS1008, doi:10.1029/2010RS004380.

Schaer, S. (1999), Mapping and predicting the Earth's ionosphere using the Global Positioning System, PhD thesis, Univ. Bern, Switzerland.

Zumberge, J. F., M. B. Heflin, D. C. Jefferson, M. M. Watkins, and F. H. Webb (1997), Precise point positioning for the efficient and robust analysis of GPS data from large networks, *J. Geophys. Res.*, *102*, 5005–5017, doi:10.1029/96JB03860.

Zus, F., G. Dick, J. Douša, and J. Wickert (2015a), Systematic errors of mapping functions which are based on the VMF1 concept, *GPS Solut.*, *19*, 277–286, doi:10.1007/s10291-014-0386-4.

Zus, F., G. Dick, S. Heise, and J. Wickert (2015b), A forward operator and its adjoint for GPS slant total delays, *Radio Sci.*, *50*, 393–405, doi:10.1002/2014RS005584.

Zus, F., Z. Deng, S. Heise, and J. Wickert (2017), Ionospheric mapping functions based on electron density fields, *GPS Solut.*, *21*, 873–885, doi:10.1007/s10291-016-0574-5.